DOI: https://doi.org/10.15407/pmach2024.04.006

UDC 621.43.056

ENHANCEMENT OF AEROENGINE COMBUSTION CHAMBER AIR COOLING HOLES DESIGN FOR EMISSION REDUCTION AND PATTERN FACTOR CONTROL

Masoud Hajivand
m.hajivand82@gmail.com
ORCID: 0000-0002-9990-9761

National Aerospace University "Kharkiv Aviation Institute"
17, Vadyma Manka str., Kharkiv, 61070, Ukraine

The results of a comprehensive numerical analysis of temperature uniformity and NO_x and CO emission predictions in an aeroengine annular combustor liner, conducted by geometrical modifications through design changes in primary cooling air, including effusion cooling holes, are shown in the paper. A total of five geometric configurations were studied using computational fluid dynamics (CFD) simulations in ANSYS CFX. The adopted combustion model was sort of a combination of the finite-rate (i.e., chemistry, chemical processes) and eddy dissipation model (FRC/EDM). Further, the combustion of liquid kerosene ($C_{10}H_{22}$) with air, subsequent to the evaporation of fuel droplets, was simulated, and the Rosin-Rammler droplet size distribution was used in spray modeling for accurate depiction of fuel atomization. Both thermal and prompt formation mechanisms of NOx were considered, while k-ε model for turbulence was adapted to capture the nature of emission. An annular combustion chamber of realistic dimensions with a double radial air swirler was modelled in 3D CAD to undertake this study for good, tangible results. Built contour plots allowed to analyze the temperature distribution and NO_x concentration along the axis from the center of the injector. Charts on the pattern factor, temperature, and NO_x and CO concentrations at the outlet of the combustor served as performance metrics. The simulation was implemented with a two-step chemical kinetics scheme for kerosene combustion with the P1 radiation model, which would give an accurate thermal radiation prediction. One of the major objectives of this research is to compare the CFD results at the combustor outlet with gas dynamic and thermodynamic calculations that have been carried out using AxStream software at the Department of Aeroengine Design, Kharkiv Aviation Institute. It is important to emphasize that the mean deviation of gas dynamic results obtained from AxStream and CFD simulation results was found to be insignificant, hence the CFD approach has been validated. The results testify that redesigning the combustor liner, especially in the design related to primary and effusion cooling holes, drastically reduced NO_x and CO emissions. Also, these design modifications have helped in reducing or improving temperature uniformity at the combustor outlet, either way enhancing combustion efficiency and performance.

***Keywords**: combustion chamber, cooling air, pattern factor, emission, NO_x formation, CFD.*

Introduction

Gas turbine combustor design is a complicated, multidisciplinary task since it will be necessary to balance a large number of design objectives carefully: emission minimization, maintaining low pressure losses, stability of the combustion process, and optimization of uniformity for thermodynamic properties of the gas outflow, including temperature distribution. These tasks are to be carried out by experimental and numerical methods; this presupposes long-time-consuming iterative procedures. Engineers must carefully conduct numerical simulations, as they rely on the assumptions of mathematical models and a profound comprehension of the phenomena. One of the key challenges in combustor design is maintaining a proper balance among these sometimes-conflicting demands. For instance, a better temperature profile at the combustor exit – which would allow to increase the life of turbine vanes – homogenizes the hot gases through more intense mixing and hence can increase pressure drop across the liner. However, the total pressure loss must be minimized because every one percent increase in pressure loss can have a strong influence on fuel efficiency or thrust [1]. Besides, another key problem is the NO_x emission reduction since NO_x is created at high temperatures during the combustion process of hydrocarbon fuels such as natural gas, oil, and coal. In general, the following three major techniques have been employed to reduce NO_x emissions, including reducing peak temperatures in the combustion zone, shortening the gas residence time at high temperatures, and decreasing oxygen concentration [2].

Several technological solutions, like Water-Steam Injection, Rich Burn Quick Quench Lean Burn (RQL), and Lean Direct Injection (LDI), were developed to apply these methods in modern aircraft gas tur-

bines. Simulation of the internal flow dynamics of a real aircraft engine combustor is a very challenging task as it incorporates phenomena such as turbulent mixing, liquid fuel atomization, swirling motions, and a host of chemical reactions. Modern computational techniques, such as Large Eddy Simulation (LES), hold promise for more accurate representations of these phenomena. Still, they remain computationally intensive and are not affordable yet for routine design purposes [3]. Less accurate but more commonly used RANS simulations have manageable computational requirements and thus find wide acceptance for design purposes. Success in the combustion design optimization using CFD has been demonstrated in various studies. For example, nitric oxide emission reduction in the combustor design was achieved through CFD analysis by Koutsenko et al., and, to give another example, Rudolph et al. also came up with a CFD process that could give rapid combustor performance evaluation using fuel injector data and CAD geometry [4, 5]. Further, Constantinescu et al. and Jiang et al. demonstrated that LES had better prediction capability than RANS in turbulence and combustion simulations, but that LES, while fairly complex, had yet to find its way into everyday applications.

Various studies have used both numerical and experimental methods to test the performance of effusion cooling and air dilution in gas turbine combustors. In [6], Zong et al. compare different numerical models for angled effusion cooling holes in a micro-gas turbine combustor. They found that the adiabatic model overestimates the discharge coefficient and is less accurate for wall cooling effectiveness predictions but comparably performs adequately with the CHT model on near-wall flow prediction. Its accuracy improved with respect to the film thickness and velocity, increasing in the flow direction angle. Ji et al. [7] conducted an experimental and numerical research to evaluate the impact of 30°, 90°, and 150° cooling hole angles in lean burn conditions. They observed that backward injections increase the general cooling, especially at high coolant flow rates, while vertical jets disrupt the main flow and result in decreased heat transfer to the liner. Wang et al. [8] conducted a study of the cooling hole inclination angle in a Can-type aircraft gas turbine combustor. In this study, the 30° was proved to yield the best cooling performance, and the liner temperature was reduced by 31.7% because of the most uniform temperature distribution. Pang et al. [9] analyzed the role of the cooling hole diameters concerning outlet temperature distribution and found that larger diameters increased high-temperature regions and reduced uniformity, decreasing combustion efficiency. However, multi-inclined cooling holes with a diameter of 0.5 mm gave the most uniform outlet temperature with the highest combustion efficiency. Ding et al. [10] conducted experimental studies on a triple swirler combustor to explore the influence of primary and secondary dilution air jets on performance. They concluded that the location of primary dilution holes was very effective for ignition and lean blowout stability and found its optimal position to be 0.9 H downstream from the dome. Besides, the pattern factor was influenced by the arrangement of secondary dilution holes, for which design *A* proved to be better as compared to design B in a triple swirler combustor.

Research purpose

The purpose of this research is to enhance the design of aeroengine combustors, focusing specifically on the cooling air holes in the liner, including effusion cooling holes across five design cases on the annular aeroengine combustion chamber using computational fluid dynamics (CFD). These cases examine adjustments to the placement of primary cooling holes and modifications to the liner design to enhance temperature uniformity and minimize emissions. The research aims to achieve a more uniform temperature distribution at the combustor outlet, reduce emissions of nitrogen oxides (NO_x) and carbon monoxide (CO), and improve the temperature management of the liner walls. By refining these aspects, the research seeks to enhance both the pattern factor and environmental performance of the combustion chamber.

The role of governing equation and *k*–ε turbulence model in simulation of combustion phenomena

The governing equations of combustion phenomena are deduced from the basic laws of physics, namely the conservation of mass, momentum, and energy. Those are the pillars on which CFD simulations base any feasibility of accuracy in the behavior of both fuel and air during combustion. In fact, real combustion processes, which generally contain turbulence, require more equations in order to take into consideration such complexity of interactions between flow turbulence and the combustion process. In this paper, the flow conditions have been solved by a standard k–ε model of turbulence. This model is one of the most widely used turbulence models in industry due to its good balance between computational efficiency and capability to give reasonably accurate results for a wide range of turbulent flows. In other words, it gives emphasis to the following two properties of turbulence, namely: Turbulent kinetic energy, *k*, which represents the energy

the turbulent eddies possess; turbulent dissipation rate, ε, which describes the rate with which this turbulent energy is transferred into heat or lost by viscosity. The equations governing these properties of turbulence were derived starting from the Reynolds-averaged Navier-Stokes (RANS) equations in which the turbulent fluctuations are averaged in time. Unlike the algebraic models described before, the k–ε model solves two additional partial differential equations: one for the turbulent kinetic energy k and another for its dissipation rate ε. Both variables are fundamental in the computation of turbulence intensity and the scale of turbulent structures within the flow, which enables a more accurate forecast of how turbulence will interact with chemical reactions in combustion.

Although a whole array of turbulence models has been developed, tailored to flow conditions and levels of complexity, the high Reynolds number *k*–ε model has proved rather robust in applications involving high-speed, turbulent flows typical of industrial and aeroengine combustion chambers.

Two-equation models, such as the *k*-ε model, are significantly less expensive in terms of computational resource compared to advanced models like RSMs or LES, which need substantially greater resources for solving multiple turbulence equations or even transient turbulent structures, especially in turbulent combustion. The balance between simplicity and effectiveness makes the k-ε model quite ideal for industrial applications, such as gas turbines and aeroengines. It gives reliable results while remaining computationally feasible for large-scale simulations.

However, it is to be kept in mind that the standard k-ε model assumes isotropy of turbulence. This is a valid assumption for most flows; however, it does not fully develop the complexities of anisotropic turbulence that may appear in cases such as swirling flows or near-wall regions. Nevertheless, this model has undergone numerous validations and applications in a large number of investigations and research projects. The latter makes it a widely accepted tool for use in engineering and research applications.

Its roots have been understood to go back to work done by Launder and Spalding, 1974; whose formulations remain a backbone for most modern turbulence modeling. These equations, modified and improved over time, provided the backbone for numerous successful CFD projects. It indeed proved that the basis was applicable for a wide spectrum of flows, including reacting flows.

The mathematical model of combustion process and NOx formation

In this study, we employed a combined Finite Rate Chemistry (FRC) and Eddy Dissipation Model (EDM) to simulate combustion processes, integrated in ANSYS CFX [11]. This approach calculates the reaction rates separately for each model – Finite Rate Chemistry and Eddy Dissipation –then selects the minimum rate between the two. This procedure is implemented for every reaction step individually, allowing different steps of the combustion process to be influenced either by chemical kinetics or turbulent mixing, depending on the local conditions. For example, one reaction step may be governed by slow chemical kinetics, on the other hand another might be controlled by faster turbulent mixing, all at the same physical location.

This flexibility also extends to multi-step reaction schemes, where different combustion models can be applied to different reaction steps within the same simulation, enhancing the model's variety. Predefined reaction schemes often take advantage of this feature, regardless of the global model selected.

The combined Finite Rate Chemistry/Eddy Dissipation model is robust across a wide range of turbulent flow conditions and is particularly effective for reactions spanning low to high Damköhler numbers, where the rate of chemical reactions can be either slower or faster than the turbulent mixing timescale. This makes it ideal for complex combustion conditions, where different parts of the domain might have different limiting factors. In regions where turbulent mixing controls the reaction rate, the Eddy Dissipation Model excels, while in zones where chemical kinetics dominate, the Finite Rate Chemistry model takes precedence [11].

Magnussen and Hjertager proposed the eddy dissipation model (EDM) [12], which is based on Spalding's [13] theory that the reaction rate is dictated by the mixing process or the rate of eddy breakdown.

The Eddy Dissipation model works best for turbulent flows with a high chemical reaction rate relative to the flow's transport processes. There is no kinetic control over the reaction process. Thus, ignition and processes in which chemical kinetics limit reaction rate may be difficult to anticipate [11]. This turbulence-chemistry interaction model is based on the findings of [12]. The smaller of the two expressions below represents the net rate of production for species *i* due to reaction *r*

$$R_{i,r} = \nu_{i,r} M_{\omega,i} A \rho \frac{\varepsilon}{k} \min\left(\frac{Y_R}{\nu_{R,r} M_{\omega,R}} \right); \quad (1)$$

$$R_{i,r} = \nu_{i,r} M_{\omega,i} AB \rho \frac{\varepsilon}{k} \min\left(\frac{\sum_p Y_p}{\sum_j^N \nu_{j,r} M_{\omega,j}} \right), \quad (2)$$

where Y_R is the mass fraction of a particular reactant R, Y_p is the mass fraction of any product species P and A, B are empirical constants equal to 4, 0.5 respectively.

The Finite Rate Chemistry (FRC) model in ANSYS CFX is based on the notion that the rate of progress for an elementary reaction, indicated as reaction k, may only be reversible if the equivalent reverse reaction is explicitly described. This technique enables a more accurate description of chemical kinetics, particularly in complex combustion processes, where forward and backward reactions influence the total reaction dynamics. The rate of progress for reaction k, which governs how swiftly a reaction proceeds, is then determined using the following formula

$$\overline{R}_{i,r} = (\nu'_{i,r} - \nu''_{i,r}) \left[k_{f,r} \prod_{j=1}^{N} [C_{i,r}]^{\eta'_{j,r}} - k_{b,r} \prod_{j=1}^{N} [C_{j,r}]^{\eta''_{j,r}} - \right], \quad (3)$$

where N – is the number of chemical species in the system; $\nu'_{i,r}$ – is the stoichiometric coefficient for reactant i in reaction r; $\nu''_{i,r}$ – is the stoichiometric coefficient for product i in reaction r; $k_{f,r}$ – is the forward rate constant for reaction r and $k_{b,r}$ is the backward rate constant for reaction r; $C_{i,r}$ – is the molar concentration of species j in reaction r; $\eta'_{j,r}$ – is the rate exponent for reactant species j in reaction r; $\eta''_{j,r}$ – is the rate exponent for product species j in reaction r.

In ANSYS CFX, the built-in formula for determining the forward and backward rate constants relies on the Arrhenius temperature dependency. This technique presupposes that the rate of a chemical reaction varies exponentially with temperature, which is given by the Arrhenius equation. Specifically, the rate constants are determined using the following formula

$$F_k = B_k = A_k T^{\beta_k} \exp\left(\frac{E_k}{RT} \right), \quad (4)$$

where A_k is pre-exponential factor; β_k is the temperature exponent (dimensionless); E_k is the activation energy; T is the absolute temperature [13].

In gas flames over 1800 K, the predominant source of NO_x is the prevalence of N and O radicals. Thermal NO, or Zeldovich NO (named after Y. B. Zeldovich, 1946, who proposed the mechanism), is generated through elementary reactions (Baulch et al. 1994) [14].

Nitric oxide (NO) is generated through the interaction of free radical oxygen and nitrogen species, which are prevalent at elevated temperatures. The Zeldovich mechanism, a two-step process, is thought to predominate in the (R_1) and (R_2) reactions [11]. Under sub-stoichiometric or near-stoichiometric conditions, a tertiary reaction may be significant, as seen in reaction (R_3).

When reaction (R_3) is included with the previous two, it is referred to as the extended Zeldovich mechanism. The term "thermal" is employed because the activation energy of the initial reaction is significantly high, attributable to the robust triple bond in N_2 molecules, rendering the reaction sufficiently rapid only at elevated temperatures [14].

The first reaction is the rate limiting phase of the thermal NO production. The reaction rates (R_1, R_2, R_3) are delineated beneath each respective reaction.

$$O + N_2 \xrightarrow{k_1} NO + N; \quad k_1 = (1.8 \cdot 10^{11}) \exp\left(-\frac{38370}{T} \right); \quad \text{R } (R_1)$$

$$O + N_2 \xrightarrow{k_2} NO + N; \quad k_2 = (6.4 \cdot 10^{9}) \exp\left(-\frac{3162}{T} \right); \quad (R_2)$$

$$O + N_2 \xrightarrow{k_3} NO + N; \quad k_3 = 3.0 \cdot 10^{3}. \quad (R_3)$$

When multiplied by the concentrations of the reactants, they yield rates in terms of [kmol/m^3/s], which can be converted to a volumetric mass source term [11].

$$\frac{d[\mathrm{NO}]}{dt} = k_1[\mathrm{O}][\mathrm{N}_2] + k_2[\mathrm{N}][\mathrm{O}_2] + k_3[\mathrm{N}][\mathrm{OH}]. \quad (5)$$

Because:

$$\frac{d[\mathrm{NO}]}{dt} = k_1[\mathrm{O}][\mathrm{N}_2] - k_2[\mathrm{N}][\mathrm{O}_2] - k_3[\mathrm{N}][\mathrm{OH}] \quad (6)$$

As described in ANSYS CFX Solver Theory Guide [11], the thermal formation in kg/m^3/s, $S_{\mathrm{NO,\,thermal}}$, is therefore related to the rate of Reaction (R_1)

$$S_{\mathrm{NO,thermal}} = 2W_{\mathrm{NO}}k_{\mathrm{thermal}}[\mathrm{O}][\mathrm{N}_2];\ k_{\mathrm{thermal}} = k_1. \quad (7)$$

Here, represents the molecular mass of NO. Thus, provided the molar concentrations [O] and [N_2] of O radicals and N_2 are known, the thermal NO mechanism can be estimated [11].

Prompt formation of NO occurs when temperatures are lower than 1800 K. Hydrocarbon flames typically contain NO concentrations that are too high to be explained by Zeldovich mechanisms. Hydrocarbon radicals can react with molecular nitrogen to form HCN, which may be oxidized to NO under lean flame conditions.

$$\mathrm{CH} + \mathrm{N}_2 \rightarrow \mathrm{HCN} + \mathrm{N}; \quad (R_4)$$

$$\mathrm{HCH} + \mathrm{O}_2 \rightarrow \mathrm{NO} + \ldots. \quad (R_5)$$

The full mechanism is pretty intricate. However, De Soete (see also Peters and Weber, 1991) proposed a single reaction rate to represent the NO source by the Fenimore mechanism, here we have $S_{\mathrm{NO,\,prompt}}$

$$S_{\mathrm{NO,prompt}} = W_{\mathrm{NO}}k_{\mathrm{prompt}}[\mathrm{O}_2]^{1/2}[\mathrm{N}_2][\mathrm{Fuel}]\left(\frac{w}{\rho}\right)^{3/2}; \quad (8)$$

$$k_{\mathrm{prompt}} = A_{\mathrm{prompt}}\exp(-T_{A,\mathrm{prompt}}/T). \quad (9)$$

Here W_{NO} and w denote molar mass of NO and the mean molar mass of the mixture, respectively. The Arrhenius coefficients depend on the fuel [11].

When modeling NO_x formation in kerosene/air combustion, the thermal NO and prompt NO are taken into account.

During the CFD simulation, we solve the mass transport equation for NO species, taking into consideration convection, diffusion, NO generation and consumption, and associated species. This approach is entirely generic, stemming from the fundamental principle of mass conservation. For thermal and quick NO_x processes, the following NO species transport equation is sufficient [15]

$$\rho\frac{\partial Y_{\mathrm{NO}}}{\partial t} + \rho u_i\frac{\partial Y_{\mathrm{NO}}}{\partial x_i} = \frac{\partial}{\partial x_i}\left(\rho D\frac{\partial Y_{\mathrm{NO}}}{\partial x_i}\right) + S_{\mathrm{NO}}. \quad (10)$$

he source term S_{NO} is to be determined for different NO_x formation mechanism.

The 3D CAD model of annular combustion chamber and the mesh strategy for the CFD simulation

The 3D CAD model of the annular combustion chamber of the turbofan aeroengine SaM-146 [16], which is shown in (Fig. 1, a) and (Fig. 1, b), was created using SOLIDWORKS 2020 [17], a widely used software for CAD and CAM applications. This model was based on the actual geometric parameters of the SaM-146 engine prototype, as provided by the department of aeroengine design at the Kharkiv aviation institute. This precise modeling allowed for an accurate representation of the combustion chamber for CFD analysis.

It is crucial to note that Figure (Fig. 1, a) displays turbine stators within the model; however, these stators do not reflect the precise geometric details of the actual turbine stator blades. Instead, their inclusion is intended solely to illustrate the general configuration of the combustion chamber in relation to the stators. Although these stators were incorporated into the CFD simulation, the primary focus of the analysis is on the critical parameters at the combustor outlet, not on the stators themselves.

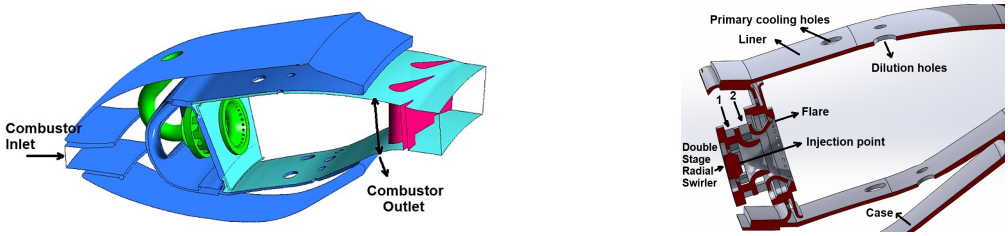

a b

Fig. 1. 3D CAD model of SaM-146 combustion chamber:
a – 20-degree sector of combustion chamber with a visual geometry of stators;
b – the cross section with swirler and liner details; 1 and 2 – primary and secondary stage of radial swirler

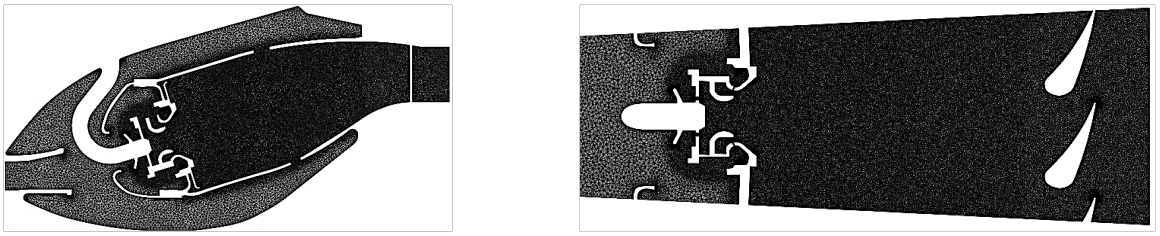

a b

Fig. 2. Unstructured tetrahedral mesh:
a – side view; b – view from above

The design of this type of combustion chamber has been the subject of extensive research, including studies by S. Roux, M. Cazalens and T. Poinsot [18] and Férand, M et.al [19]. Due to the complex geometry of the combustion chamber, an unstructured mesh was employed in this simulation as shown in Fig. 2, consisting of approximately 23 million elements. This approach allows for greater flexibility in accurately capturing intricate flow details within the chamber, ensuring better resolution of critical areas in the combustion process such as NO and CO formation capture.

Boundary condition regulation for CFD simulation from obtained gas dynamic results from AxStream

Dhanush Kumar used advanced software tools, including AxCycle™ for thermodynamic simulations and the AxSTREAM® platform developed by SoftInWay Inc [20], to design and analyze the engine's compressor, combustion chamber, and turbine operating parameters in his Master degree project for this engine prototype [21]. These tools were useful in performing the thermo-gas dynamic calculations [21], which ensured that the engine's performance parameters were predicted correctly. By including these methods into the examination, we were able to lay a strong foundation for the CFD simulations, yielding reliable data for future analysis and refinement of the SaM-146 engine's combustion chamber characteristics.

This comprehensive method emphasizes the necessity of incorporating both theoretical and practical tools into engine design, ensuring that CFD simulations closely match real-world engine behavior and various operational conditions.

Table 1. Boundary condition regulations

Parameters	Dhanush Kumar [21]	This Study (CFD)
Air total temperature, K	864.330	863.275
Air static temperature, K	854.680	854.684
Total pressure, kPa	2928.27	2928.19
Static pressure, kPa	2815.43	2816.69
Axial velocity, m/s	135.320	138.757
Mach number	0.23	0.24
Air mass flow rate, kg/s	2.40	2.38
Fuel mass flow rate, kg/s	0.048	0.032
Temperature of fuel, K	373.15	373.15

Table 1 shows the results and most essential boundary conditions from Dhanush Kumar's gas dynamic calculations in his master's degree project [21], which were used to create the boundary conditions for this inquiry and CFD modeling.

By aligning the boundary condition parameters from Kumar's gas dynamic calculations –specifically through critical engine components such as the high-pressure compressor outlet to the combustion chamber inlet and compressor outlet [21] –with those used in the CFD simulation, we can effectively implement the combustion CFD model. This alignment ensures consistency between theoretical and simulated approaches, resulting in more reliable and accurate predictions of combustion behavior.

Comparing the results obtained in gas dynamic calculations in AxStream with CFD results at the combustion chamber outlet

By merging the data from the thermo-gas dynamic calculations implemented by Kumar [21] with the capabilities of ANSYS CFX, the study was able to strengthen the accuracy of the simulation findings, ensuring a more trustworthy forecast of important operating parameters in this research. This approach underlines the necessity of leveraging both pre-calculated data and solver changes in CFD modeling to get exact, validated outcomes.

Table 2 displays the critical characteristics at the output of the combustion chamber, which were previously computed by Dhanush Kumar [21] and then compared with the results obtained from this CFD analysis. These parameters include temperature, axial velocity, Mach number, total pressure, and static pressure. The comparison demonstrates that the majority of the variations between the pre-calculated data with AxStream and the CFD results are within acceptable bounds, with the mean variances being around 5%. However, the Mach number exhibited a higher variance of 15.45%, which is considerably larger than the other metrics.

Table 2. The obtained results at the combustor exit by gas dynamics calculation of Dhanush Kumar and CFD simulation in this study

Parameters	Dhanush Kumar [473]	This Study (CFD)	Mean Deviation
Air total temperature, K	1508.00	1535.66	-1.83%
Air static temperature, K	1503.00	1531.84	-1.91%
Total pressure, kPa	2681.255	2624.600	2.11%
Static pressure, kPa	2657.04	2595.98	2.3%
Axial velocity, m/s	88.49	89.14	-0.73%
Mach Number	0.110	0.127	-15.45%

Research of 5 variously designed combustion chamber liners considering the primary cooling and effusion hole design

Base Case – The base case is shown in Fig. 3 with primary and dilution holes.

First case (displacement) – According to the base case, primary cooling holes were repositioned 10 mm towards the combustion primary zone on the liner, as shown in Fig. 3.

Second case (displacement) – According to the base case, primary cooling holes were repositioned 20 mm towards the combustion primary zone on the liner, as shown in Fig. 3.

Third case (modification) – Fig. 4 clearly illustrates the adjustment and modifications made to the combustion chamber liner. The liner's internal monitor was extended by roughly 48 mm into the dilution zone upstream of the combustor. This extension serves as a flame stabilizer, facilitating consistent burning, and also affects airflow dynamics within the combustion chamber.

Alongside this extension, 18 effusion apertures, each approximately 2 mm in diameter, were integrated into the liner. The perforations are deliberately positioned to cool both the expanded monitor and the liner walls, thereby improving the system's thermal management. This design guarantees that the liner can endure the extreme temperatures in the combustion chamber, enhancing longevity and efficiency.

Fig. 4 also shows the principal alteration to the primary cooling holes. This modification implements customized walls surrounding the primary cooling holes to enhance the regulation of cooling air penetration into the combustion chamber. This modification regulates the entry of cooling air into the combustion zone, enhancing the cooling process and facilitating temperature management, which in turn improves emissions and overall performance, including pattern factor.

The general view of the combustion chamber liner, including its cross section, is shown in Fig. 5. This image shows a complete perspective on the liner's overall design, showing critical elements such as the extended internal monitor, effusion holes, and principal cooling hole adjustments. By viewing the cross section, the internal structure of the liner and the layout of the cooling systems can be easily understood, affording vital insight into how the liner handles airflow and heat dispersion within the combustor.

Fourth case (adding effusion cooling holes) – A total of 18 effusion cooling holes, each with a diameter of 1.5 mm, were placed to the liner to reduce its temperature and manage the pattern factor. These effusion holes were strategically located 3 mm downstream from the redesigned primary cooling holes, toward the dilution zone, as shown in Fig. 6. Effusion cooling is a highly effective technology [22, 23, 24, 25, 26] utilized in aeroengine combustion chambers to give better thermal protection. By allowing a thin layer of cooling air to flow through several small holes, effusion cooling forms a protective barrier between the hot combustion gases and the liner surface, considerably reducing the thermal load on the liner.

After the simulation was conducted in ANSYS CFX, all critical parameters were thoroughly analyzed. This included the temperature distribution within the combustion chamber, predictions of nitrogen oxides (NO_x) and carbon monoxide (CO) emissions, as well as the pattern factor and the temperature contour on the liner wall. These parameters are vital for assessing the performance and environmental impact of the combustor.

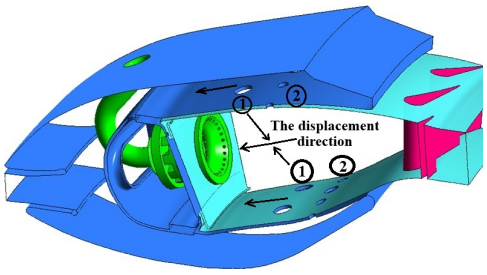

Fig. 3. The base case:
1 –primary cooling holes; 2 – dilution holes

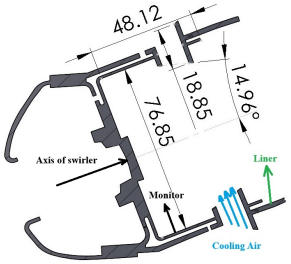

Fig. 4. The modification of combustor liner as a third case. All the geometrical parameters above are in mm

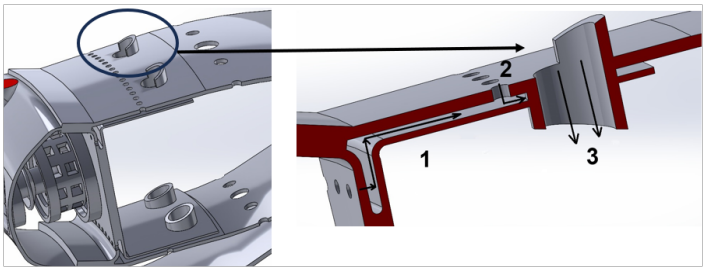

a b

Fig. 5. The modification of combustor liner:
a – liner 3D CAD modeling; b – the cross section of medicated line;
1 – extended monitor; 2 – effusion cooling holes;
3 – the modification of primary cooling holes

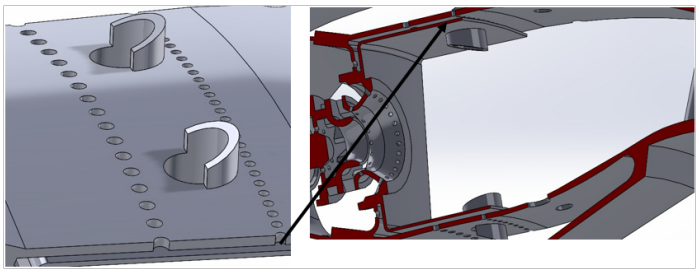

a b

Fig. 6. The 3D CAD model of Forth case of modification:
a – adding effusion cooling holes;
b – the cross section of liner with the location of the second row of effusion cooling holes as in the fourth case

Results and discussion

Before analyzing obtained results, it should be mentioned that the combustion reaction of Jet A with air is modeled by a single species surrogate. A two-step global mechanism for Jet A ($C_{12}H_{23}$) is employed, which consists in a first step for fuel oxidation into CO and H_2O, and a second step for CO oxidation into CO_2

$$C_{12}H_{23}+11.75\ O_2 \rightarrow 12\ CO_2+11.5\ H_2O \qquad (R_6)$$

$$CO+0.5\ O_2 \rightarrow CO_2 \qquad (R_7)$$

Arrhenius coefficients for this scheme can be found in [27].

As shown in Fig. 7, a, the maximum temperature in the base case is 2570 K. For the first and second cases, shown in Fig. 7, b and Fig. 7, c, where the primary cooling holes were repositioned towards the primary combustion zone, the maximum temperatures are 2500 K and 2570 K, respectively. Besides that, Fig. 7, d and Fig. 7, e show the temperature contours for the modified third and fourth cases, which have maximum temperatures of 2580 K and 2570 K, respectively.

The temperature contours in these modified cases reveal that the maximum temperature is concentrated around the swirler and liner monitor, primarily due to the high recirculation zone formed in the primary combustion zone. This recirculation zone enhances flame stability but also results in localized areas of intense heat.

Moreover, it is evident that the rate of air penetration through the modified cases (third and fourth) is higher compared to the base, first, and second cases.

This increased airflow is clearly visible in the top-down views in Fig. 8, d and Fig. 8, e, where the modified cases demonstrate a higher rate of air mixing, while Figs. 8, a, b, and c show maximum temperatures of 2580 K, 2500 K, and 2570 K, respectively.

It is worth noting that in the base, first, and second cases, the maximum wall temperatures of the combustor liner are concentrated around the regions just after the primary cooling holes, as shown in Fig. 9, a, b, and c. The maximum wall temperatures in these cases are 2003 K, 1998 K, and 2080 K, respectively.

The simulation results for these cases indicate that repositioning the primary cooling holes towards the core of the primary combustion zone, where both velocity and temperature are high, leads to flame overstretching. This overstretching can destroy the flame structure, causing overheating of various and key components like the liner walls and the high-pressure turbine stators, potentially leading to damage or a reduced lifespan of the combustion chamber.

In contrast, as seen in Fig. 9, d and Fig. 9, e, the redesigned liner with extra effusion cooling holes (third and fourth cases) displays more effective thermal management and a more uniform temperature distribution over the combustor walls. The highest wall temperatures in these circumstances are 2064 K and 2103 K, respectively. In the third situation (Fig. 9, d), high temperatures still occur around the primary cooling holes. However, by adding a second row of effusion cooling holes after the primary cooling holes, this high-temperature zone is effectively minimized, as demonstrated in Fig. 9, e. This suggests that the additional effusion holes have a substantial role in improving the cooling efficiency and minimizing localized overheating, resulting in enhanced thermal protection for the liner and combustor components.

As shown in Fig. 10, a, and Fig. 10, b, the maximum NO formation in terms of mass fraction is 0.00202 and 0.0011, respectively.

This indicates that by repositioning the primary cooling holes 10 mm closer to the combustion primary zone, the mass fraction of NO is reduced so this reduction is primarily due to the increased penetration of cooling air into the hotter regions of the flame, effectively lowering the local flame temperature, which directly reduces thermal NOx formation.

However, Fig. 10, c shows a different scenario where the primary cooling holes were moved 20 mm towards the combustion primary zone. In this case, the penetration of the cooling air destroys the critical recirculation zone that stabilizes the flame, leading to flame stretching. This phenomenon, as previously discussed, can severely compromise the integrity of turbine stators and blades. The NO formation in this case is no longer uniform, with a maximum value of 0.0011 concentrated near the liner surfaces in the dilution zone, indicating that the cooling air is not optimally interacting with the flame to reduce NO uniformly across the combustion zone.

For the modified cases (third and fourth), depicted in Fig. 10, d and Fig. 10, e, there is a notable reduction in NO formation within the primary combustion zone.

This is attributed to the more effective penetration of cooling air into the liner, as well as the regulation of the high recirculation zone in these regions. The introduction of additional effusion holes significantly improves the cooling effect, stabilizing the flame and reducing peak temperatures that contribute to NO formation.

In the third case, shown in Fig. 10, d, the maximum mass fraction of NO is reduced to 0.0007, while in the fourth case (Fig. 10, e), the maximum NO formation is 0.0009. These lower NO concentrations reflect the enhanced cooling efficiency and flame stability achieved in the modified designs, ensuring that the combustion process is both cleaner and more stable compared to the base and first cases.

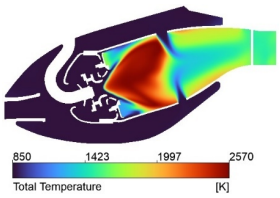

a

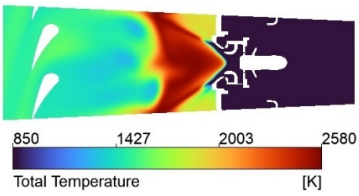

a

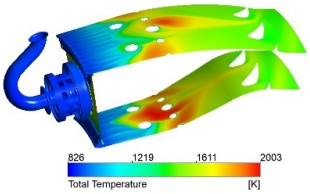

a

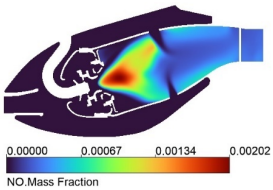

a

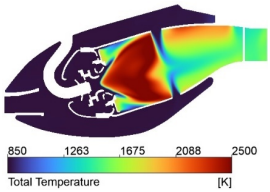

b

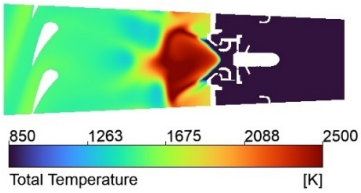

b

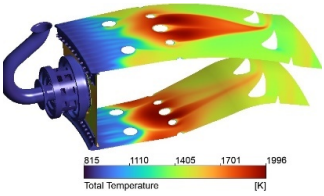

b

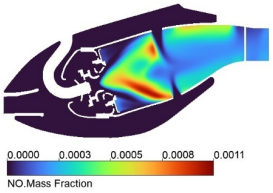

b

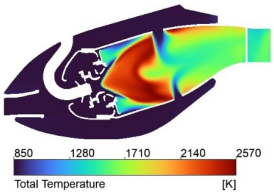

c

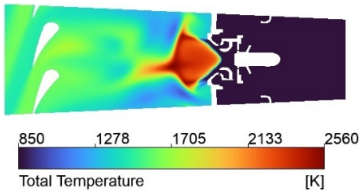

c

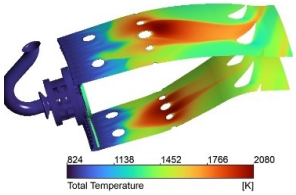

c

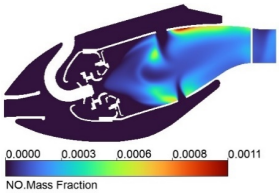

c

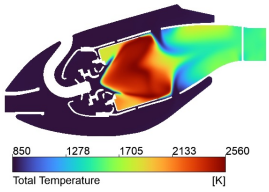

d

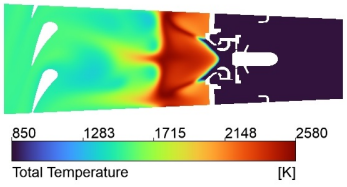

d

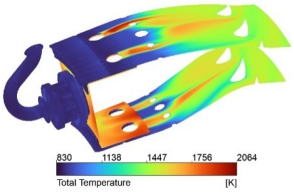

d

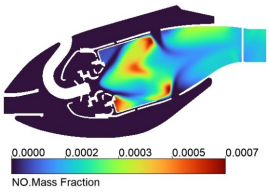

d

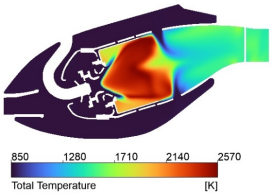

e

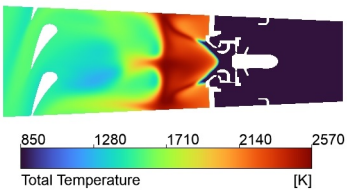

e

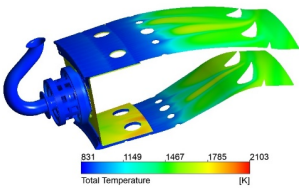

e

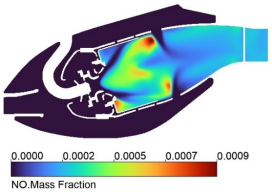

e

Fig. 7. Temperature distribution along the middle plane of combustor:
a – base case;
b – first case;
c – second case;
d – third case;
e – fourth case

Fig. 8. Temperature distribution along the middle plane of combustor, view from above:
a – base case;
b – first case;
c – second case;
d – third case;
e – fourth case

Fig. 9. Temperature distribution on the wall surfaces of combustor:
a – base case;
b – first case;
c – second case;
d – third case;
e – fourth case

Fig. 10. NO distribution along the middle plane of combustor:
a – base case;
b – first case;
c – second case;
d – third case;
e – fourth case

Compared to the base case (0.00202) along the middle plane of the combustion chamber, NO formation in the first case is reduced by 45.5%, decreasing from 0.00202 to 0.0011. Similarly, the second case also shows a 45.5% reduction, lowering NO formation to 0.0011. In the third case, the reduction is more significant at 65.3%, bringing NO formation down to 0.0007. The fourth case shows a 55.4% decrease, reducing NO formation to 0.0009.

These percentage reductions highlight the significant improvement in NO emissions, particularly in the third and fourth modified cases, where cooling efficiency and flame stability have been optimized.

The maximum total temperature at the combustor outlet, as shown in Fig. 11, a for the base case is 1912.45 K, while the first case shows a 10.1% increase (2106.05 K), and the second case shows a 9.5% increase (2094.23 K).

For the third case, there is a 5.0% reduction (1816.43 K), and for the fourth case, there is a 4.8% reduction (1821 K) compared to the base case.

The repositioning of the primary cooling holes in the first and second cases leads to higher outlet temperatures, which is likely due to insufficient cooling air mixing in these configurations. In contrast, the addition of effusion holes in the third and fourth cases including the primary cooling holes modification results in a more effective cooling mechanism, bringing down the outlet temperature.

For the minimum total temperature at the outlet, the base case shows 1420.76 K. In the first case, there is a 3.2% decrease (1375.94 K), while the second case shows a 6.7% reduction (1325.46 K). The third case shows the largest reduction of 13.4% (1229.62 K), and the fourth case has a reduction of 3.5% (1371.24 K). These reductions indicate improved cooling in the modified cases, especially in the third case, which shows the strongest cooling effect in the minimum temperature values.

The exit temperature distribution of a gas turbine combustor plays a critical role in determining the durability of turbine blades and vanes. A more uniform exit temperature profile contributes to extending the operational life of these components by minimizing thermal stress and reducing the risk of localized overheating. To quantify the uniformity of this temperature distribution, a parameter known as the pattern factor (PF) is introduced [61].

Pattern factor (PF) is defined as a measure of the non-uniformity of the exit temperature profile, and it is calculated as follows [61]

$$PF = \frac{T_{\max} - T_{\text{mean}}}{T_{\text{mean}} - T_{\text{inlet}}}, \quad (11)$$

where, $T_{\max}$, T_{mean} and T_{inlet} are the combustor maximum exit temperature, average exit temperature, and inlet temperature, respectively.

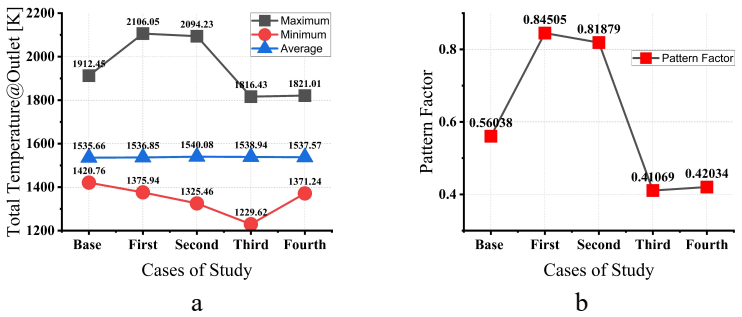

a b

Fig. 11. Obtained results:
a – maximum, minimum and average total temperature at the combustor outlet;
b –pattern factor

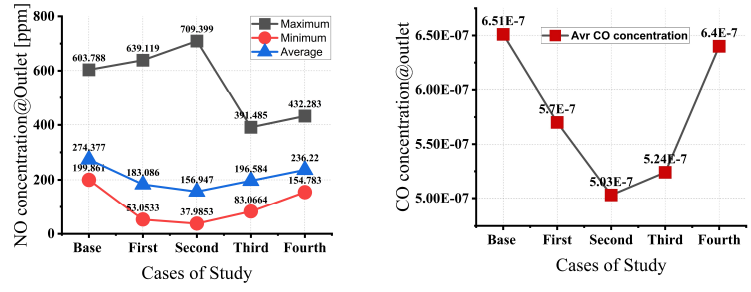

a b

Fig. 12. Obtained results:
a – maximum, minimum and average NO formation at the combustor outlet;
b – average formation of CO at the combustor outlet

The pattern factor, as displayed in Fig. 11, b, for the base case is 0.56038. In the first case, there is a significant 50.8% increase (0.84505), and in the second case, there is a 46.1% increase (0.81879). However, the third and fourth cases show marked improvements, with the third case showing a 26.7% reduction (0.41069) and the fourth case showing a 25% reduction (0.42034). This reflects that the modifications in the first and second cases resulted in greater temperature gradients and poorer uniformity, while the addition of effusion cooling holes and the modification of primary cooling holes in the third and fourth cases improved temperature distribution, achieving better uniformity.

Regarding NO formation (Fig. 12, a), the base case has a maximum NO formation of 603.788 ppm. The first case shows a 5.8% increase (639.119 ppm), while the second case shows a 17.5% increase (709.399 ppm). In the third case, however, NO formation is reduced by 35.2% (391.485 ppm), and in the fourth case – by 28.4% (432.283 ppm). The NO reduction in the third and fourth cases is significant, reflecting the improved cooling by effusion holes, which reduces peak flame temperatures and thereby limits thermal NOx formation. The average NO formation follows a similar pattern, with reductions of 33.3%, 42.7%, 28.4%, and 13.9% for the first, second, third, and fourth cases, respectively, compared to the base case.

For CO mass fraction (Fig. 12, b), the base case shows an average mass fraction of 6.51×10^{-7}. In the first case, CO formation is reduced by 12.4% (5.7×10^{-7}), and in the second case – by 22.7% (5.03×10^{-7}). However, in the third case, the CO mass fraction is reduced by 19.5% (5.24×10^{-7}) compared to the base case, while the fourth case shows a slight increase of 1.7% (6.4×10^{-7}). The reductions in the first and second cases are due to the higher combustion temperatures, which lead to more complete combustion and lower CO formation. The increase in CO in the fourth case is likely due to localized cooling, leading to incomplete combustion in certain areas.

The modifications lead to varying degrees of enhancement. For temperature, the first and second cases show higher temperatures due to disrupted cooling, while the third and fourth cases show improvements due to the introduction of effusion holes and primary cooling holes modification. Pattern factor improvements are significant in the third and fourth cases, reflecting better temperature uniformity. NO reduction is substantial in the third and fourth cases, while CO reduction is most effective in the first and second cases, though the third case also shows good results with minor CO reductions.

To illustrate the cooling air penetration in the liner of the combustion chamber, streamlines were implemented for the base and fourth cases, as shown in Fig. 13, a and Fig. 13, b.

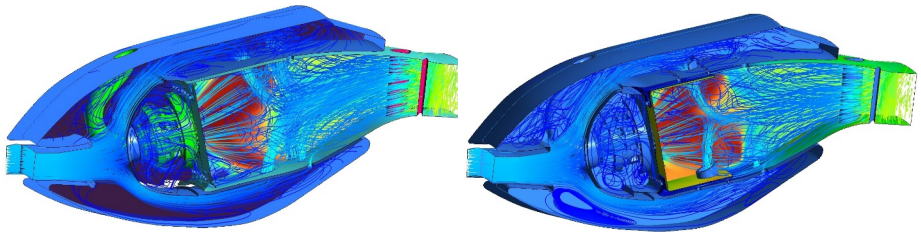

a b

Fig. 13. Internal flow streamlines:
a – base case; b – fourth case (modified)

According to Fig. 13, a, the streamlines for the base case reveal how cooling air flows through the primary and secondary cooling holes. The streamlines indicate a relatively dispersed flow pattern with less effective cooling near the liner, leading to uneven temperature distribution and localized hot spots. This uneven cooling can result in higher peak temperatures and increased NO_x formation due to less efficient thermal management.

Fig. 13, b displays the streamlines for the fourth case, which includes modifications to the primary cooling holes and the addition of effusion cooling holes.

The streamlines for this case show a significantly improved cooling air penetration. The modified primary cooling holes are repositioned to enhance cooling efficiency by directing the airflow more effectively towards high-temperature regions. The inclusion of effusion cooling holes further refines the cooling air distribution, resulting in a more uniform and controlled cooling effect across the liner surface. The improved streamlines in this case indicate better penetration and distribution of cooling air, leading to a more uniform temperature distribution, reduced maximum temperatures, and lower NO_x emissions.

The visual comparison of these streamlines highlights the effectiveness of the modifications made in the fourth case. The optimized primary cooling holes new design and the addition of effusion cooling holes contribute to a more efficient cooling process, enhancing overall combustor performance and thermal management.

In Fig. 14, a and Fig. 14, b, the cooling air penetration for both the base and fourth cases is shown, including the vectors of cooling air entering the liner. These vectors visually demonstrate how the cooling air flows into the combustion chamber liner. In the base case (Fig. 14, a), the cooling air vectors show a less concentrated and less controlled penetration pattern, resulting in uneven cooling and areas of high thermal stress. Conversely, in the fourth case (Fig. 14, b), with the modified primary cooling holes and added effusion cooling holes, the vectors display a more streamlined and directed air penetration. This leads to enhanced cooling efficiency and better temperature regulation within the liner.

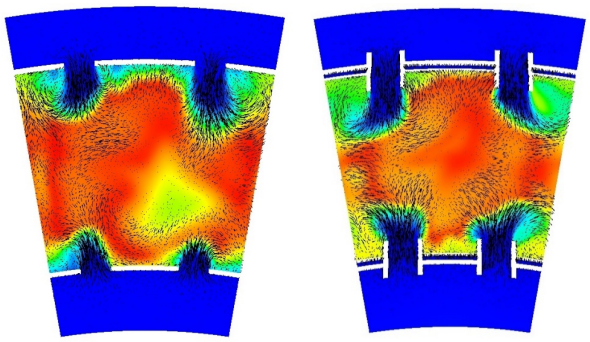

a b

Fig. 14. The cooling air penetration vectors in the primary cooling air:
a – base case; b – fourth case (modified)

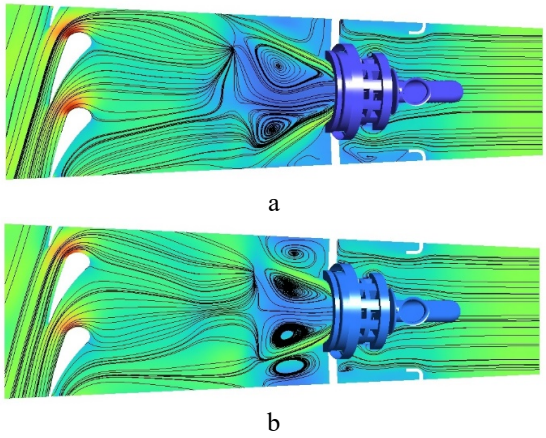

a

b

Fig. 15. The stream line, view from the above:
a – base case; b – fourth case (modified)

In Fig. 15, a and Fig. 15, b, streamlines are shown for both the base and fourth cases to depict the generation of the recirculation zone, as previously mentioned. In the base case (Fig. 15, a), the streamlines reveal a less structured airflow pattern, which can lead to less effective flame stabilization and poor mixing, contributing to less uniform combustion and higher peak temperatures.

However, in the fourth case (Fig. 15, b), the streamlines indicate a more controlled and efficient generation of the recirculation zone. The enhanced cooling air penetration, along with the improved airflow pattern, helps in stabilizing the flame and creating a more uniform temperature distribution within the combustion chamber, contributing to better overall performance and reduced NOx formation.

Conclusion

Numerical CFD investigation in ANSYS CFX revealed that the variation of geometric combustion chamber liner, in design of primary cooling holes, and addition of effusion cooling jets overwhelmingly improved the aeroengine annular combustion chamber characteristics. This resulted in a more uniform temperature distribution (pattern factor), increasing the cooling efficiency at the liner. These improvements directly reduced NOx and CO emissions; in the optimal variants, NOx reached a reduction of up to 65.3% at the combustion chamber outlet. The research further validated the CFD method by comparing the obtained results with gas dynamic calculations using AxStream software, which was implemented in the Kharkiv Aviation Institute department of aeroengine design for dependable and accurate results. Out of the five configurations, case three and case four showed the best results by optimizing liner and primary combustion zone cooling strategies with enhancements in pattern factor and achieving better NOx management.

References

1. Lefebvre, A. H. & Ballal, D. R. (2010). Gas Turbine Combustion: Alternative Fuels and Emissions. Third Edition. CRC Press, 557 p. https://doi.org/10.1201/9781420086058.
2. (1999). Nitrogen oxides: Pollution prevention and control. In: Pollution Prevention and Abatement Handbook 1998: Toward Cleaner Production. World Bank Publications, p. 245–249. https://www.ifc.org/content/dam/ifc/doc/1990/handbook-nitrogen-oxides-pollution-prevention-and-control.pdf.
3. Watanabe, H., Kurose, R., Yano, Y., Makino, H., & Komori, S. (2012). Numerical simulation of soot formation in spray jet flames. *Journal of the Society of Powder Technology, Japan*, vol. 49, iss. 6, pp. 467–477. https://doi.org/10.4164/sptj.49.467.
4. Koutsenko, I. G., Onegin, S. F., & Sipatov, A. M. (2004). Application of CFD-based analysis technique for design and optimization of gas turbine combustors. Proceedings of the ASME Turbo Expo 2004: Power for Land, Sea, and Air (June 14–17, 2004, Vienna, Austria), vol. 1: Turbo Expo 2004, pp. 253–260. https://doi.org/10.1115/GT2004-53398.
5. Dudebout, R., Reynolds, B., & Molla-Hosseini, K. (2004). Integrated process for CFD modeling and optimization of gas turbine combustors. Proceedings of the ASME Turbo Expo 2004: Power for Land, Sea, and Air (June 14–17, 2004, Vienna, Austria), vol. 1: Turbo Expo 2004, pp. 679–686. https://doi.org/10.1115/gt2004-54011.

6. Zong, C., Ji, C., Cheng, J., & Zhu, T. (2022). Comparison of adiabatic and conjugate heat transfer models on near-wall region flows and thermal characteristics of angled effusion cooling holes. *Thermal Science and Engineering Progress*, vol. 30, article 101269. https://doi.org/10.1016/j.tsep.2022.101269.
7. Ji, Y., Ge, B., & Zang, S. (2022). Analysis of effusion cooling under realistic swirl reacting flow in gas turbine combustor. *Applied Thermal Engineering*, vol. 216, article 119101. https://doi.org/10.1016/j.applthermaleng.2022.119101.
8. Wang, J., Hu, Z., Du, C., Tian, L., & Baleta, J. (2021). Numerical study of effusion cooling of a gas turbine combustor liner. *Fuel*, vol. 294, article 120578. https://doi.org/10.1016/j.fuel.2021.120578.
9. Pang, L., Zhao, N., Xu, H., Li, Z., Zheng, H., & Yang, R. (2023). Numerical simulations on effect of cooling hole diameter on the outlet temperature distribution for a gas turbine combustor. *Applied Thermal Engineering*, vol. 234, article 121308. https://doi.org/10.1016/j.applthermaleng.2023.121308.
10. Ding, G., He, X., Zhao, Z., An, B., Song, Y., & Zhu, Y. (2014). Effect of dilution holes on the performance of a triple swirler combustor. *Chinese Journal of Aeronautics/Chinese Journal of Aeronautics*, vol. 27, iss. 6, pp. 1421–1429. https://doi.org/10.1016/j.cja.2014.10.008.
11. (2015). ANSYS CFX-Solver Theory Guide, Release 16.2. ANSYS, Inc.
12. Magnussen, B. F. & Hjertager, B. H. (1977). On mathematical modeling of turbulent combustion with special emphasis on soot formation and combustion. *Symposium (International) on Combustion*, vol. 16, iss. 1, pp. 719–729. https://doi.org/10.1016/s0082-0784(77)80366-4.
13. Spalding, D. B. (1977). Development of the eddy-break-up model of turbulent combustion. *Symposium (International) on Combustion*, vol. 16, iss. 1, pp. 1657–1663. https://doi.org/10.1016/s0082-0784(77)80444-x.
14. Warnatz, J., Maas, U., & Dibble, R. (2006). Combustion: Physical and Chemical Fundamentals, Modeling and Simulation, Experiments, Pollutant Formation. Springer Berlin, Heidelberg, 378 p. https://doi.org/10.1007/978-3-540-45363-5.
15. Jiang, B., Liang, H., Huang, G., & Li, X. (2006). Study on NOx formation in CH4/air jet combustion. *Chinese Journal of Chemical Engineering*, vol. 14, iss. 6, pp. 723–728. https://doi.org/10.1016/S1004-9541(07)60002-0.
16. *PowerJet SaM146*. Wikipedia. https://en.wikipedia.org/wiki/PowerJet_SaM146.
17. 3D CAD Design Software. SolidWorks: official site. https://www.solidworks.com/.
18. Roux, S., Cazalens, M., & Poinsot, T. (2008). Outlet-boundary-condition influence for large eddy simulation of combustion instabilities in gas turbines. *Journal of Propulsion and Power*, vol. 24, no. 3, pp. 541–546. https://doi.org/10.2514/1.33739.
19. Férand, M., Livebardon, T., Moreau, S., & Sanjosé, M. (2019). Numerical prediction of far-field combustion noise from aeronautical engines. *Acoustics*, vol. 1, iss. 1, pp. 174–198. https://doi.org/10.3390/acoustics1010012.
20. SoftInWay. Identity Server. (n.d.). https://resources.softinway.com/.
21. Kumar, D. (2020). Turbofan engine for medium-range aircraft with take-off thrust 101.46kN. Ph. D. Thesis. http://dx.doi.org/10.13140/RG.2.2.35715.32802.
22. Andreini, A., Becchi, R., Facchini, B., Picchi, A., & Peschiulli, A. (2017). The effect of effusion holes inclination angle on the adiabatic film cooling effectiveness in a three-sector gas turbine combustor rig with a realistic swirling flow. *International Journal of Thermal Sciences*, vol. 121, pp. 75–88. https://doi.org/10.1016/j.ijthermalsci.2017.07.003.
23. Arcangeli, L., Facchini, B., Surace, M., & Tarchi, L. (2008). Correlative Analysis of Effusion Cooling Systems. *Journal of Turbomachinery*, vol. 130, iss. 1, article 011016, 7 p. https://doi.org/10.1115/1.2749298.
24. Rhee, D. H., Choi, J. H., & Cho, H. H. (2003). Flow and heat (mass) transfer characteristics in an impingement/effusion cooling system with crossflow. *Journal of Turbomachinery*, vol. 125, iss. 1, pp. 74–82. https://doi.org/10.1115/1.1519835.
25. Scrittore, J. J., Thole, K. A., & Burd, S. W. (2007). Investigation of velocity profiles for effusion cooling of a combustor liner. *Journal of Turbomachinery*, vol. 129, iss. 3, pp. 518–526. https://doi.org/10.1115/1.2720492.
26. Shrager, A. C., Thole, K. A., & Mongillo, D. (2018). Effects of effusion cooling pattern near the dilution hole for a double-walled combustor liner – Part 1: Overall effectiveness measurements. *Journal of Engineering for Gas Turbines and Power*, vol. 141, iss. 1, article 011022, 10 p. https://doi.org/10.1115/1.4041148.
27. Valachovic, T. G. (1993). Numerical predictions of idle power emissions from gas turbine combustors. Proceedings of the ASME 1993 International Gas Turbine and Aeroengine Congress and Exposition (May 24–27, 1993, Cincinnati, Ohio, USA), vol. 3A: General, article V03AT15A026, 10 p. https://doi.org/10.1115/93-GT-175.

Received 18 September 2024

Удосконалення конструкції отворів повітряного охолодження камери згоряння авіаційного двигуна для зменшення викидів і контролю рівномірності температури

M. Hajivand

Національний аерокосмічний університет ім. М. Є. Жуковського «Харківський авіаційний інститут»,
61070, Україна, м. Харків, вул. Вадима Манька, 17

Поточне дослідження є комплексним числовим аналізом, що стосується рівномірності температури та прогнозування викидів NO_x і CO в жаровій трубі кільцевої камери згоряння авіаційного двигуна шляхом геометричних модифікацій, зокрема зміни конструкції первинного охолоджувального повітря, включаючи отвори для ефузійного охолодження. Було досліджено п'ять геометричних конфігурацій із використанням моделювання CFD в ANSYS CFX. Прийнята модель горіння поєднувала хімію з кінцевою швидкістю реакції та модель вихрової дисипації (FRC/EDM). Крім того, моделювалося згоряння рідкого гасу (C12H23) з повітрям після випаровування паливних крапель. Моделювання розпилення використовувало розподіл розмірів крапель Розіна-Раммлера для точного відображення процесу розпилення палива. Було розглянуто як термічні, так і миттєві механізми утворення NO_x, тоді як для турбулентності використовувалася модель k-ε. Кільцева камера згоряння реалістичних розмірів із подвійним радіальним завихрювачем повітря була змодельована в 3D CAD для проведення цього дослідження з хорошими, надійними результатами. Контурні графіки розподілу температури та концентрації NO_x аналізувалися вздовж осі від центру інжектора. Діаграми рівномірності температури та концентрацій NO_x і CO на виході з камери згоряння слугували показниками продуктивності. Моделювання було реалізовано за допомогою двоетапної схеми хімічної кінетики для згоряння гасу та моделі випромінювання P1, яка забезпечила точне прогнозування теплового випромінювання. Однією з основних цілей цього дослідження було порівняння результатів CFD на виході з камери згоряння з газодинамічними та термодинамічними розрахунками, виконаними за допомогою програмного забезпечення AxStream на кафедрі конструкції авіаційних двигунів Харківського авіаційного інституту. Важливо зазначити, що середнє відхилення результатів газодинаміки, отриманих із результатів моделювання AxStream і CFD, було незначним, що підтвердило правильність підходу CFD. Результати свідчать про те, що перепроєктування жарової труби камери згоряння, зокрема конструкцій, пов'язаних із первинними та ефузійними охолоджувальними отворами, значно скоротило викиди NO_x і CO. Крім того, ці конструктивні зміни допомогли знизити або покращити рівномірність температури на виході з камери згоряння, що підвищило ефективність і продуктивність згоряння.

***Ключові слова**: камера згоряння, охолоджувальне повітря, фактор рівномірності, викиди, формування NO_x, CFD.*

Література

1. Lefebvre A. H., Ballal D. R. Gas Turbine Combustion: Alternative Fuels and Emissions. Third Edition. CRC Press, 2010. 557 p. https://doi.org/10.1201/9781420086058.
2. Nitrogen Oxides: Pollution Prevention and Control. In: Pollution Prevention and Abatement Handbook 1998: Toward Cleaner Production. World Bank Publications, 1999. P. 245–249. https://www.ifc.org/content/dam/ifc/doc/1990/handbook-nitrogen-oxides-pollution-prevention-and-control.pdf.
3. Watanabe H., Kurose R., Yano Y., Makino H., Komori S. Numerical simulation of soot formation in spray jet flames. *Journal of the Society of Powder Technology, Japan*. 2012. Vol. 49. Iss. 6. P. 467–477. https://doi.org/10.4164/sptj.49.467.
4. Koutsenko I. G., Onegin S. F., Sipatov A. M. Application of CFD-based analysis technique for design and optimization of gas turbine combustors. Proceedings of the ASME Turbo Expo 2004: Power for Land, Sea, and Air (June 14–17, 2004, Vienna, Austria). 2004. Vol. 1: Turbo Expo 2004. P. 253–260. https://doi.org/10.1115/GT2004-53398.
5. Dudebout R., Reynolds B., & Molla-Hosseini K. Integrated process for CFD modeling and optimization of gas turbine combustors. Proceedings of the ASME Turbo Expo 2004: Power for Land, Sea, and Air (June 14–17, 2004, Vienna, Austria). 2004. Vol. 1: Turbo Expo 2004. P. 679–686. https://doi.org/10.1115/gt2004-54011.
6. Zong C., Ji C., Cheng J., Zhu T. Comparison of adiabatic and conjugate heat transfer models on near-wall region flows and thermal characteristics of angled effusion cooling holes. *Thermal Science and Engineering Progress*. 2022. Vol. 30. Article 101269. https://doi.org/10.1016/j.tsep.2022.101269.
7. Ji Y., Ge B., Zang S. Analysis of effusion cooling under realistic swirl reacting flow in gas turbine combustor. *Applied Thermal Engineering*. 2022. Vol. 216. Article 119101. https://doi.org/10.1016/j.applthermaleng.2022.119101.
8. Wang J., Hu Z., Du C., Tian L., Baleta J. Numerical study of effusion cooling of a gas turbine combustor liner. *Fuel*. 2021. Vol. 294. Article 120578. https://doi.org/10.1016/j.fuel.2021.120578.

9. Pang L., Zhao N., Xu H., Li Z., Zheng H., Yang R. Numerical simulations on effect of cooling hole diameter on the outlet temperature distribution for a gas turbine combustor. *Applied Thermal Engineering*. 2023. Vol. 234. Article 121308. https://doi.org/10.1016/j.applthermaleng.2023.121308.
10. Ding G., He X., Zhao Z., An B., Song Y., Zhu Y. Effect of dilution holes on the performance of a triple swirler combustor. *Chinese Journal of Aeronautics/Chinese Journal of Aeronautics*. 2014. Vol. 27. Iss. 6. P. 1421–1429. https://doi.org/10.1016/j.cja.2014.10.008.
11. ANSYS CFX-Solver Theory Guide, Release 16.2. ANSYS, Inc. 2015.
12. Magnussen B. F., Hjertager B. H. On mathematical modeling of turbulent combustion with special emphasis on soot formation and combustion. *Symposium (International) on Combustion*. 1977. Vol. 16. Iss. 1. P. 719–729. https://doi.org/10.1016/s0082-0784(77)80366-4.
13. Spalding D. B. Development of the eddy-break-up model of turbulent combustion. *Symposium (International) on Combustion*. 1977. Vol. 16. Iss. 1. P. 1657–1663. https://doi.org/10.1016/s0082-0784(77)80444-x.
14. Warnatz J., Maas U., Dibble R. Combustion: Physical and Chemical Fundamentals, Modeling and Simulation, Experiments, Pollutant Formation. Springer Berlin, Heidelberg, 2006. 378 p. https://doi.org/10.1007/978-3-540-45363-5.
15. Jiang B., Liang H., Huang G., Li X. Study on NOx formation in CH4/air jet combustion. *Chinese Journal of Chemical Engineering*. 2006. Vol. 14. Iss. 6. P. 723–728. https://doi.org/10.1016/S1004-9541(07)60002-0.
16. *PowerJet SaM146*. Wikipedia. https://en.wikipedia.org/wiki/PowerJet_SaM146.
17. 3D CAD Design Software. SolidWorks: official site. https://www.solidworks.com/.
18. Roux S., Cazalens M., Poinsot T. Outlet-boundary-condition influence for large eddy simulation of combustion instabilities in gas turbines. *Journal of Propulsion and Power*. 2008. Vol. 24. No. 3. P. 541–546. https://doi.org/10.2514/1.33739.
19. Férand M., Livebardon T., Moreau S., Sanjosé M. Numerical prediction of far-field combustion noise from aeronautical engines. *Acoustics*. 2019. Vol. 1. Iss. 1. P. 174–198. https://doi.org/10.3390/acoustics1010012.
20. SoftInWay. Identity Server. (n.d.). https://resources.softinway.com/.
21. Kumar D. Turbofan engine for medium-range aircraft with take-off thrust 101.46kN. Ph. D. Thesis. 2020. http://dx.doi.org/10.13140/RG.2.2.35715.32802.
22. Andreini A., Becchi R., Facchini B., Picchi A., Peschiulli A. The effect of effusion holes inclination angle on the adiabatic film cooling effectiveness in a three-sector gas turbine combustor rig with a realistic swirling flow. *International Journal of Thermal Sciences*. 2017. Vol. 121. P. 75–88. https://doi.org/10.1016/j.ijthermalsci.2017.07.003.
23. Arcangeli L., Facchini B., Surace M., Tarchi L. Correlative Analysis of Effusion Cooling Systems. *Journal of Turbomachinery*. 2008. Vol. 130. Iss. 1. Article 011016. 7 p. https://doi.org/10.1115/1.2749298.
24. Rhee D. H., Choi J. H., Cho H. H. Flow and heat (mass) transfer characteristics in an impingement/effusion cooling system with crossflow. *Journal of Turbomachinery*. 2003. Vol. 125. Iss. 1. P. 74–82. https://doi.org/10.1115/1.1519835.
25. Scrittore J. J., Thole K. A., Burd S. W. Investigation of velocity profiles for effusion cooling of a combustor liner. *Journal of Turbomachinery*. 2007. Vol. 129. Iss. 3. P. 518–526. https://doi.org/10.1115/1.2720492.
26. Shrager A. C., Thole K. A., Mongillo D. Effects of effusion cooling pattern near the dilution hole for a double-walled combustor liner – Part 1: Overall effectiveness measurements. *Journal of Engineering for Gas Turbines and Power*. 2018. Vol. 141. Iss. 1. Article 011022. 10 p. https://doi.org/10.1115/1.4041148.
27. Valachovic T. G. Numerical predictions of idle power emissions from gas turbine combustors. Proceedings of the ASME 1993 International Gas Turbine and Aeroengine Congress and Exposition (May 24–27, 1993, Cincinnati, Ohio, USA). 1993. Vol. 3A: General. Article V03AT15A026. 10 p. https://doi.org/10.1115/93-GT-175.